11th International Renewable Energy Storage Conference, IRES 2017, 14-16 March 2017, Düsseldorf, Germany

Impacts on load distribution and ageing in Lithium-ion home storage systems

Thorsten Grün[*], Kevin Stella, Olaf Wollersheim

Karlsruhe Institute of Technology (KIT), INT-PCE, Hermann-von-Helmholtz-Platz 1, Gebäude 276, 76344 Eggenstein-Leopoldshafen, Germany

Abstract

In parallel cell circuits within Lithium-ion home storage systems, the components of the circuit have an enormous influence on the load distribution and as consequence on the battery lifetime. Quality spreads within a batch of cells exist also as deviation in the connection quality. This paper presents the impacts of the system components on the load distribution and the ageing in parallel-connected circuits for exemplary module designs of commercial available home storage systems. Experimental and simulated studies show high deviations between the performances and lifetimes of several systems due to the circuit design.

Keywords: Lithium ion; battery module; analysis; modeling; topology; cycle ageing

1. Introduction

Energy storage plays an important role in the energy supply, as soon as the installed capacity of renewable energy, like photovoltaic (PV) with intermittent power, exceeds certain levels. Modern lithium ion (Li-ion) battery systems are able to deal with the challenges posed by the use in stationary storage applications.
A Li-ion battery system is an ensemble of modules, which are in turn made up of a defined number of individual cells being serial and/or parallel (XsYp) connected to each other. Battery modules, composed of low-priced cylindrical cells with average capacities of 2-3 Ah are very common in commercial home storage systems. Herein it

---
[*] Corresponding author: Tel.: +49-721-608-28282 ; fax: +49-721-608-28284
E-mail address: thorsten.gruen@kit.edu

is very comfortable for the integration in private households to stay below 48 V, which leads to a connection of several cells in parallel to aggregate the required power. In parallel circuits asymmetric load distribution can occur, which was already shown in former publications from Kamalisiahrodui et al. [1] and Bruen and Marco [2]. Reasons for asymmetric load distributions are for example unequal cell characteristics like the electrical internal cell resistance R_{cell} and the nominal capacity C_n, which was already reported by Gogoana et al. [3]. They have shown that R_{cell} can spread up to 24.7 % and C_n up to 3.6 % within a batch of 72 cells. Fleckstein et al. reported [4], that unequal temperatures within a battery module due to active cooling cause also individual ageing behavior. At least a circuit of battery cells consists, beside cells, out of the electrical resistance of the connection $R_{transfer}$ (weld, bolts…etc) and the electrical interconnection resistance R_{inter} in form of a current collector. Depending on their resistance values and the circuit design, they can affect asymmetric load distribution within parallel-connected cells and as consequence the ageing behavior of the system.

In this paper, we would like to add a new aspect on the investigation of parallel-connected cells and introduce via experiment and an electrical-thermal model, how the load distribution is determined on deviations of the chosen circuit components and the circuit design within commercial PV home storage systems. The impacts on the ageing and the performance during the operation within high fluctuated PV supply will be discussed.

2. Battery modelling

2.1. Electrical-thermal modeling

For an accurate modeling of a Li-ion battery system, it is mandatory to consider the electrical and thermal behavior of the cell and the system. Therefore we would like to present an equivalent circuit model (ECM) coupled to a thermal model.

Electrical battery models should be able to describe the electrical cell behavior and that of the battery system. In the specific case of parallel-connected cells it means the interaction between cells in terms of different State of Charges (SOC) due to a divergent load distribution, which influence the cell characteristic like the open circuit voltage (U_{OCV}) and R_{cell}. Fig. 1 presents the ECM with respect to the elements of the circuitry for two exemplary studied topologies (T1 and T2) for n parallel-connected cells.
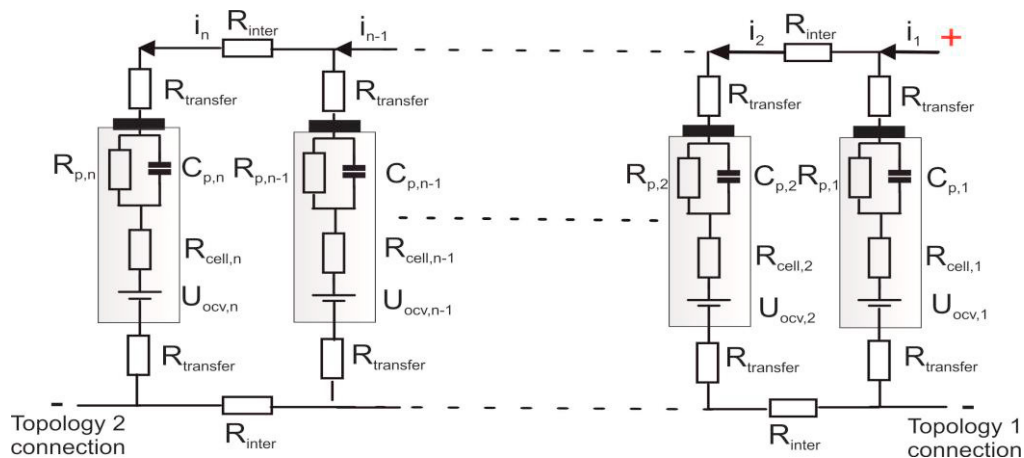

Fig. 1. ECM for n parallel-connected cells in form of two different topologies.

The circuit components R_{inter} and $R_{transfer}$ are represented in form of an ohmic resistance. Those resistances depend only on the used materials, the geometry of the current collector and also on the chosen connection technique. A summary of available ECM for single cell modeling is given by He et al. [5]. For our single cell model, we chose the Thevenin Model, which exist of U_{OCV}, R_{cell} and one RC-circuit (with R_p and C_p), which represents over-voltages U_{RC} in form of diffusion, charge transfer and double layer effects.

R_{cell} presents ohmic resistance effects caused by the electrodes, separator and the electrolyte. It depends on the cell

chemistry, the SOC, the single cell temperature T_{cell} and also on the ageing level. U_{OCV} depends on the cell chemistry and the SOC. The relationship between SOC, U_{OCV} and the partial voltage dU_{OCV}/dQ has a nonlinear characteristic, which can be implemented and simulated with a Look Up table (see also Fig. 2).

Two cell chemistries in form of commercial cylindrical cells were chosen for this study, which are 3 Ah 26650 Lithium-ion phosphate (LFP) and 2.45 Ah 18650 Lithium cobalt oxide (LCO). For those two cell chemistries R_{cell} and U_{OCV} were measured for four cells. R_{cell} was measured for several SOC by using a 0.5 C charge and discharge pulse for 20 seconds. U_{RC} was determined by using the MATLAB© Optimization Toolbox as it is reported by Huria et al. [6]. Herein an optimization algorithm is used, which fits the parameters R_P and C_P to reduce the sum square error between the measured and simulated voltage plot during the 0.5 C charge and discharge pulses.
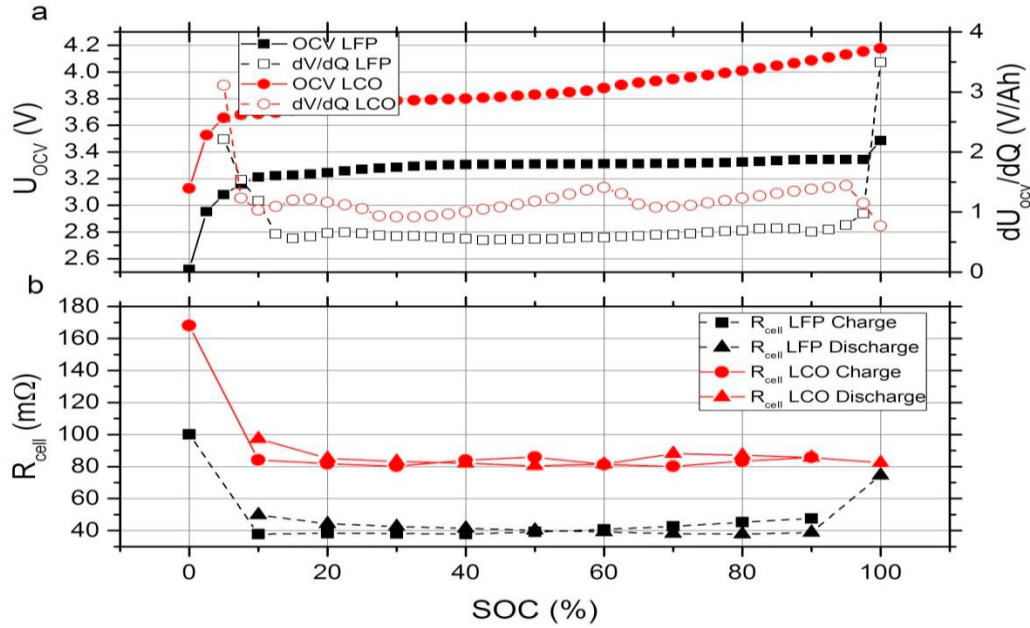

Fig. 2. (a) Measured U_{OCV} and partial dU_{OCV}/dQ for LFP and LCO cells for several SOC; (b) R_{cell} plot for charge and discharge at several SOC for LFP and LCO.

The thermal model in this work considers the electrical power loss as heat generation, which depends on the current of the single cell I_{cell}, R_{cell} and $R_{transfer}$ given by the Joule heating law.

In addition cooling effects due to convection are considered with respect to the convection area A, which is the surface area of the single cell (in our case taken from the datasheet), the temperature T_{surr} of the surrounding and the heat transfer coefficient λ. With respect to the law of energy conservation, the time depending change of the cell temperature T_{cell} due to the announced heat sources and cooling effects can be expressed like in Equ. 1, in which m is the mass of the cell and h_p the heat capacity.

$$m \cdot h_p \cdot \frac{dT_{cell}}{dt} = (R_{cell} + R_{transfer}) \cdot I_{cell}^2 - \lambda(T_{cell} - T_{surr}) \cdot A \qquad (1)$$

Adjusted to the ECM of Fig. 1, the current distribution for n parallel cells can be expressed as a dynamic linear optimization problem with constraints in matrix format. The vector $\vec{\imath}$ represents the current for each node of the circuit. Matrix $\underline{R}(t, T_{cell})$ contains the ohmic resistances of the network $R_{n,n}$ for each current path of n parallel cells. It is represented as time and temperature dependent by the relationship between R_{cell} on the temperature and the SOC. The vector $\vec{u}(t)$ includes U_{OCV} and U_{RC}. At last, contains also the total current of the system $\vec{\imath_1}$. In our problem, the matrix $\underline{R}(t, T_{cell})$ (n x n) is a square matrix, which makes it possible to calculate the solution of the vector $\vec{\imath}$ by using Cramer's rule.

$$\vec{i} \cdot \underline{R}(t, T_{cell}) = \vec{u}(t)$$

$$
\begin{pmatrix} i_1 \\ i_2 \\ \vdots \\ i_n \end{pmatrix} \cdot
\begin{bmatrix}
1 & 0 & \cdots & 0 \\
R_{1,1}(t, T_{cell,1}) & \cdots & \cdots & R_{1,n}(t, T_{cell,n}) \\
\vdots & & \ddots & \vdots \\
R_{n,1}(t, T_{cell,n}) & \cdots & \cdots & R_{n,n}(t, T_{cell,n})
\end{bmatrix}
=
\begin{pmatrix}
i_1 \\
U_{ocv,1}(t) - U_{ocv,2}(t) + U_{RC,1}(t) - U_{RC,2}(t) \\
\vdots \\
U_{ocv,n-1}(t) - U_{ocv,n}(t) + U_{RC,n-1}(t) - U_{RC,n}(t)
\end{pmatrix}
\tag{2}
$$

2.2. Ageing Model

Sauer and Wenzl presented in their work [7] a comparison of different lifetime prediction models for battery systems. We use the weighted Ah throughput model which based on the assumption that the impact of a given Ah throughput on the lifetime depends also on the details of the conditions during the Ah throughput. Deviations from the standard conditions in form of temperature and current can result in a virtual decreasing of the battery lifetime. The ageing model based on the estimation of the State of Health (SOH), which is defined as the percentage ratio between the actual available capacity C_{act} and C_n. The Begin of Life (BoL) is defined with a SOH of 100 %, whereas the End of Life (EoL) is achieved by an SOH of 80 %.

In our model we consider the temperature influence in form of the Arrhenius law and adopt a gain factor α to simulate the results of the capacity fade during a 1 C charge/discharge cycling test at several temperatures from Waldmann et al.[8] .The temperature weighting factor $w_T(t)$ accelerates the virtual ageing, if T_{cell} exceeds the temperature for standard conditions T_{SC} (assumed as 25 °C).

The influence of the current rate on the ageing was shown by Ning et al. [9] and in the study of Schuster et al. [10]. Not only the growing Ah throughput, but also higher over-voltages due to higher current rates and material stress accelerate the ageing. As we already assumed for w_T, we consider only the ageing due to current rates in form of the weighting factor w_I, if I_{cell} exceeds the maximal allowed charge/discharge current I_{SC}.
To model the capacity fading, the Ah throughput is weighted by the mentioned factors. Finally the weighted Ah throughput (QTP) can be described by integrating the current flow multiplied by the weighting factors w_T and w_I for temperature and current influence for each time step over the lifetime.

$$
w_T(t) \rightarrow
\begin{cases}
\dfrac{T_{cell}(t)}{T_{sc}} > 1; & w_T(t) = \exp\left(\alpha \cdot \dfrac{T_{cell}(t)}{T_{sc}}\right) + 1 \\[3mm]
\dfrac{T_{cell}(t)}{T_{sc}} \leq 1; & w_T(t) = 1
\end{cases}
\tag{3}
$$

$$
w_I(t) \rightarrow
\begin{cases}
\dfrac{I_{cell}(t)}{I_{sc}} > 1; & w_I(t) = \left(1 + \dfrac{I_{cell}(t)}{I_{sc}}\right) \\[3mm]
\dfrac{I_{cell}(t)}{I_{sc}} \leq 1; & w_I(t) = 1
\end{cases}
\tag{4}
$$

$$
Q_{TP}(t) = \int_{BoL}^{t} |I_{cell}(t)| \cdot w_T(t) \cdot w_I(t)\, dt
\tag{5}
$$

$$
SOH(t) = \frac{C_{act}(Q_{TP}(t))}{C_n} \cdot 100\%
\tag{6}
$$

2.3. Dimension of circuit components and deviations

In home storage systems consisting of cylindrical cells, several hundreds of cells have to be connected. From an economical point of view, welding techniques (ultrasonic, resistance welding, laser welding) are comfortable, but deviations can occur due to the process parameters (e.g. pressure, number of welding points, temperature…etc.), which influence the connection resistance $R_{transfer}$. A study of Brand et al. [11] compared several welding techniques and have shown the quality dependence due to the process parameters.

In our study we used 16 26650 LFP cells from three different brands (in sum 48 cells) and connected them with a customized nickel-strip (dimension: length 24.6 mm; thickness 0.1 mm; width 7.2 mm) by using a GN-8119H resistance spot welder. The connection resistances are measured for the positive (+) and the negative (-) pole by using four-point probes of a HIOKI 3554 battery tester with an accuracy of ±1 % and a 1 kHz AC measurement current of 150 mA. The arithmetic mean value of $R_{transfer}$ yields 0.28 mΩ with a relative standard deviation of 18 %.

Among the connection technique, the current collector is also a circuit component and its electrical resistance R_{inter} depends on the constant cross-section A_{cross}, the specific resistance ρ of the material and the length l. In general, the material for the current collector is limited by the chosen connection technique. Hence we focus in our study on nickel as material for the current collector, which is a common used material in the design of battery modules consisting of welded cylindrical cells. In our module, R_{inter} between two cells is approximately 1.7 mΩ.

$$R_{inter} = \rho \cdot \frac{l}{A_{cross}} \tag{7}$$

3. Experiment

The goal of the experimental investigations is to analyze the impacts of the circuit design, the cell chemistry and the chosen material and/or dimensions for the current collector on the load distribution in parallel cell circuits within PV home storage applications. The influence of the spread of R_{cell} and $R_{transfer}$ in form of a normal distribution shall be analyzed with the validated battery model for several circuit designs consisting of LFP and LCO. Effects of different spreads for R_{cell} and C_n on the ageing are simulated for emulated 2 kWh PV home storage systems. Herein the module exists of welded 26650 LFP and 18650 LCO cells. In all simulations of the T1 and T2 systems we assume a welded battery module ($R_{transfer}$ = 0.28 mΩ) in which a nickel-strip is used as a current collector (R_{inter} = 1.7 mΩ).

3.1. Experimental setup: Analysis of load distribution depending on circuit design during PV fluctuations

For the investigation of the load distribution within parallel-connected cells and to validate the electrical part of the battery model a test bench was used to determine the single cell load with respect to I_{cell}, T_{cell} and the energy flow Q_{cell}. In the test bench four cells are connected in parallel, in which cables in a length of approx. 65 mm and a cross-section of 1.5 mm^2 are used as $R_{transfer}$. A steel sheet (width: 17.80 mm, thickness: 0.50 mm, length: 32 mm) and a copper (Cu) bar are used as current collector between the cells. A steel sheet shall emulate the influence of materials with low electrical conductivity (e.g. nickel), which are still used based on their good weldability. In contrast copper shall emulate battery modules, which use current collectors with high cross-sections to compensate the low electrical conductivity of nickel while maintaining weldability.

The resistances of the cables, and interconnection resistances as well as the resistances of the contact springs of the cell holder are measured by using four-point probes of a HIOKI 3554 battery tester with an accuracy of ±1 % and a 1 kHz AC measurement current of 150 mA. To identify the currents for each cell, the voltage drop is measured over one of the cables of the cells by using an Agilent Keysight 3972A with an accuracy of 6 ½ - digit multimeter and gets divided by the electrical contact of the cable.

The impact on the circuit design and the chosen components of the circuitries on the load distribution within home storage applications were investigated by using measurement data of the project "SafetyFirst". Herein the power

flow within a PV home storage system with grid connection (PV 3.5 kW$_p$; C$_n$ 106 Ah; annual energy consumption 4200 kWh) were measured and dimensioned to the capacity of our studied systems. The PV fluctuation was emulated by scaling measured power data of a 10 kW PV system out of the 1 MW solar storage park at the KIT campus north.
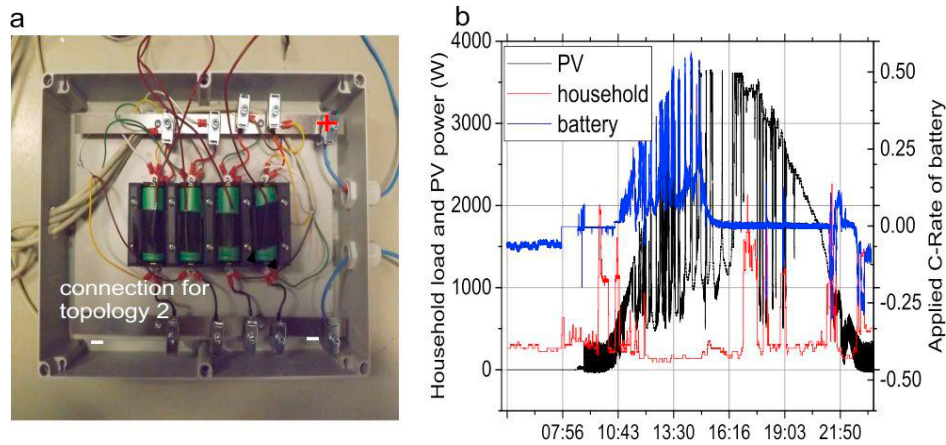

Fig. 3. (a) Test bench for emulating several circuit designs for PV home storage systems and measuring the load distribution; (b) Measured C-Rate and Power flow profile within an emulated PV home storage system with dimensioned PV power data out of a 10 kW PV system.

Table 1. List of studied systems and circuit components within the test bench of Fig. 5.

System	1	2	3	4	5	6
	LFP T1	LFP T2	LFP Cu	LCO T1	LCO T2	LCO Cu
Capacity (Ah)	12	12	12	9.8	9.8	9.8
Current collector	Steel	Steel	Cu	Steel	Steel	Cu

3.2. Simulation setup and validation of the battery model

The current running through the cells produces energy losses in the form of heat. Therefore, thermal analyses of welded cell ensembles provide an excellent independent method to study imbalances in the cell stress and to detect welding resistances of low quality. For our study two samples of four connected LFP cells in form of T1 and T2 (Fig. 1) were exposed to cycling loads according to the following CCCV (constant current constant voltage) regime: The modules were charged to the end-of-charge voltage of 3.6 V (cut-off voltage cut-off current 1/20 C with 1 C (12 A) using a BasyTec HPS battery tester. After the cut-off current is achieved, they were discharged at 1 C CC until the lower cut-off voltage of 2.0 V. During the test an infrared (IR) camera (FLIR SC 640; accuracy ± 2 %) monitors the temperature profiles of T$_{cell,1}$ and T$_{cell,4}$ for both topologies.
The electrical part of the model was validated by measurement results of the test bench of Fig. 5 for a dynamic stress test (DST). The accuracy of the battery model was validated in form of the root mean square error (RMSE) between the simulated and measured load distributions in form of I$_{cell}$ and T$_{cell}$. The maximum errors for both tests are given in Table 2.
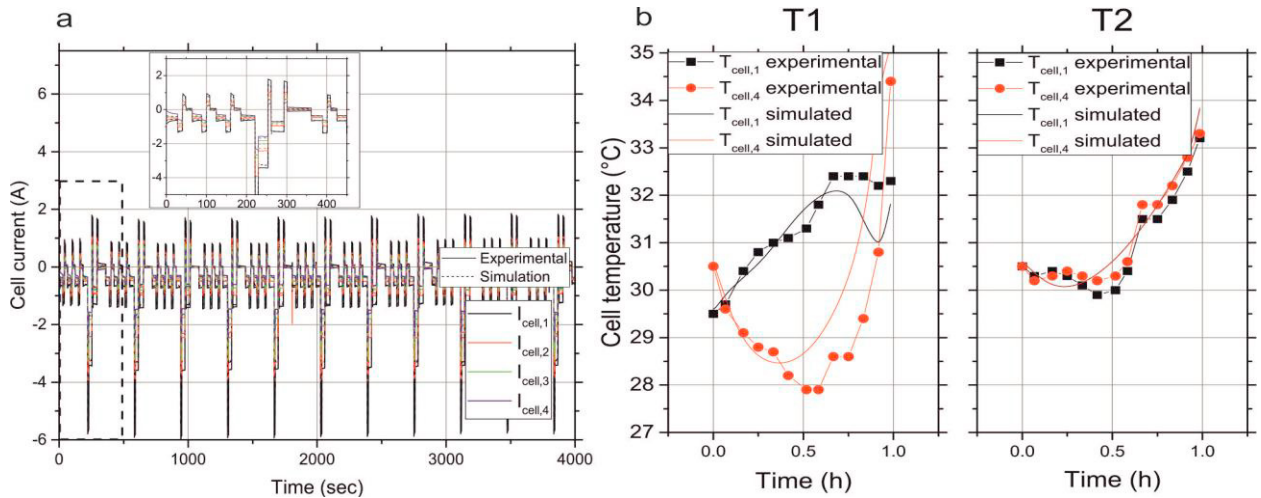
Fig. 4. Comparison of simulated and measured current and temperature distribution; (a) Shows the comparison between the measured and simulated current distribution for a LFP T1 system during a DST; (b) Represents the measured and simulated temperature profile for a 1 C CC discharge for LFP T1 and T2, which was monitored with an IR camera. The results of the RMSE are given in Table 2.

Table 2. Comparison between measured and simulated results in form of maximum RMSE.

RMSE-Max	I_{cell} (A)	Q_{cell} (Ah)	T_{cell} (°C)
DST	0.17	0.11	1.35
IR camera	-	-	1.29

4. Results

The results of the measured load distribution within emulated home storage systems are represented in form of the C-Rate for the systems of Table 1. The simulated results show the impact of spreading $R_{transfer}$ and R_{cell} depending on the number of parallel-connected cells and the circuit design on the load distribution.

The load distribution for emulated 2 kWh home storage systems with an overall voltage of 48 V (LFP: 13s16p; LCO: 11s20p) are also shown as well as their ageing behavior depending on the circuit design and quality spreads of the circuit components.

4.1. Experimental results

Fig. 5 represents the comparison of the load distribution in form of the C-Rate for the analyzed systems. The T1 systems for LFP and LCO show a very high asymmetric behavior especially during afternoons, where the PV power fluctuation are very high and get stored in the battery module. In this period, cell 1 is strained with 0.4 C whereas cell 4 is getting charged with approximately 0.2 C. The T2 systems yield a more symmetric load distribution, which is relative similar to the systems, which use Cu as current collector.
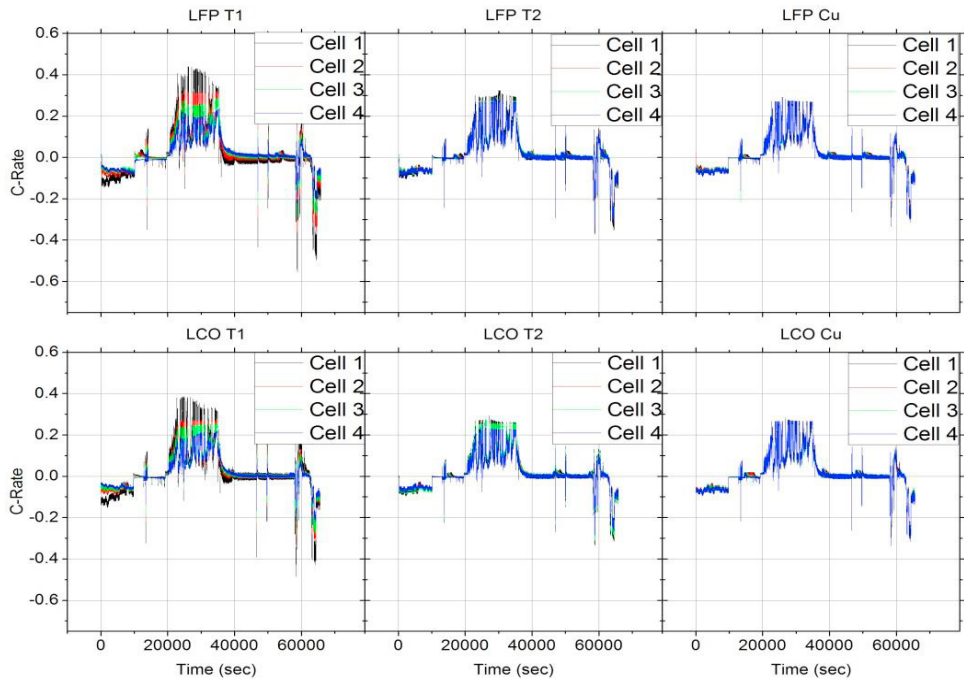
Fig. 5. Measured load distribution in form of the C-Rate for the analysed systems of Table 1.

4.2. Results of simulation

4.2.1. Impacts of spreading elemental resistances on load distribution for several systems

The influence of spreading elemental resistances ($R_{transfer}$ and R_{cell}) is analyzed for a simulated 1 C CC discharge. Herein, we calculate first the difference between I_{cell} and I_{cell}*, which is the single cell current for an ideal symmetric current distribution, for each time step. In the second step we determine the relative standard deviation of the difference between I_{cell} and I_{cell}* for the complete module and simulation time. It was done for LFP and LCO systems with increasing number of parallel cells (1s4p, 1s8p, 1s16p). A normal distribution for the resistance values were assumed with a deviation of 5 %, 10 % and 20 %.
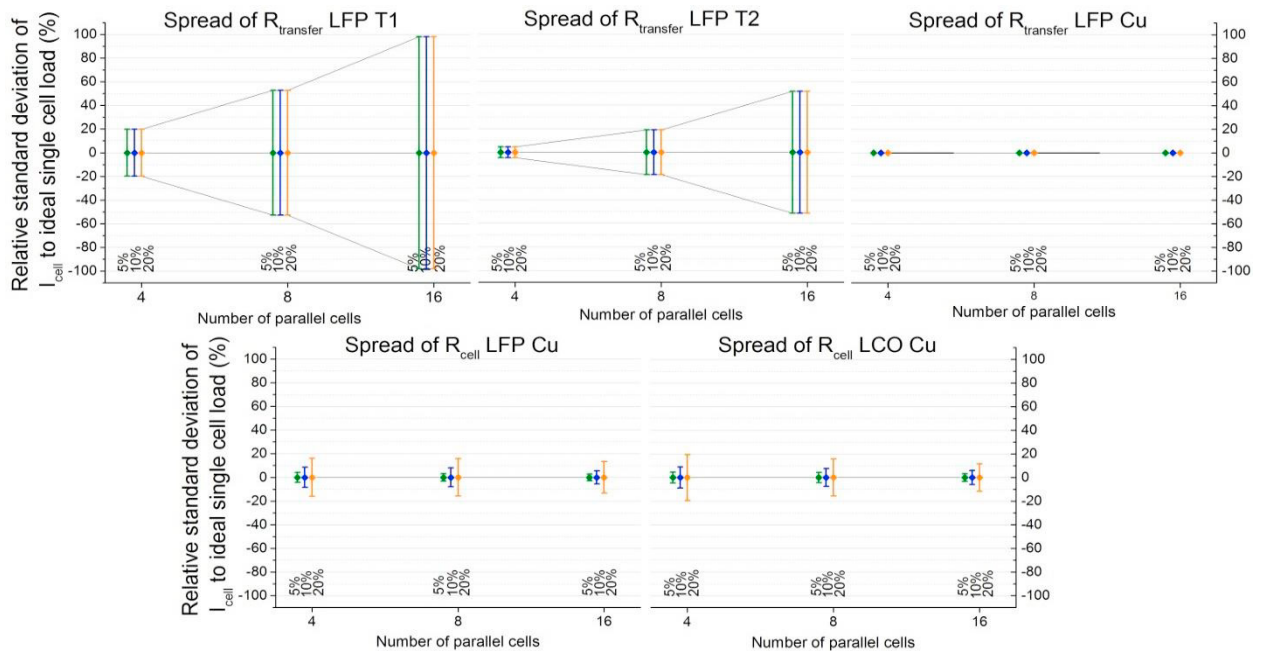
Fig. 6. Dependency of load distribution in form of the relative standard deviation of the difference of I_{cell} to the ideal cell load I_{cell}^* at normal distributed $R_{transfer}$ and R_{cell} resistances for several numbers of parallel-connected cells and systems during a simulated 1 C CC discharge.

In the LFP T1 system variations of $R_{transfer}$ have a low influence on the current distribution. The relative standard deviation of the difference between I_{cell} and the ideal cell load I_{cell}^* is for a spread of 5 -20 % the same. With increasing cell number the relative standard deviation increase from ± 20 % in a 1s4p system to ± 100 % in a 1s16p system. In the LFP T2 system the variation of $R_{transfer}$ has also a low influence on the current distribution. In this system the increasing of the cell number leads to an increasing of approx. ± 5 % in a 1s4p system to ± 50 % in a 1s16p system.

In comparison to the systems LFP T1 and LFP T2, which use nickel as current collector, the spread of $R_{transfer}$ as well as the increasing number of parallel connected cells have no influence on the load distribution in the LFP Cu system. The relative standard deviation is 0 %, which means, that the load distribution is symmetric. The spread of R_{cell} achieves a different result. Herein the load distribution in the LFP Cu and LCO Cu is asymmetric with increasing spread of R_{cell}. In terms of more parallel-connected cells, the relative standard deviation is decreasing, caused by the assumption of a normal distribution. Herein most of R_{cell} receive values similar to the mean value of R_{cell}.

4.2.2. Simulation of load distribution within emulated 2 kWh home storage systems

The simulation of the load distribution within 2 kWh home storage systems (see Fig. 7) shows that the maximum C-Rate for the LFP systems, which occurs during the fluctuation afternoons, can be reduced due to the circuit design from 2.5 C to 0.8 C. The differences in the maximum and minimum SOC in the battery system are also reduced from 69 % in the LFP T1 system to 25 % in the LFP T2 system. The maximum C-Rate of the LCO T1 system gains 1.4 C and is reduced also to 0.7 C in the LCO T2 system. The LCO T2 system design achieves nearly the ideal symmetric load distribution also. The comparison of LCO T1 and LFP T1 shows, that in general the C-Rate for the single cells is much higher in the LFP T1 system than in in the LCO T1 system. In the LFP T1 system also high fluctuations in both charge direction can be seen, whereas the discharge C-Rates for the LCO T1 system are very low.
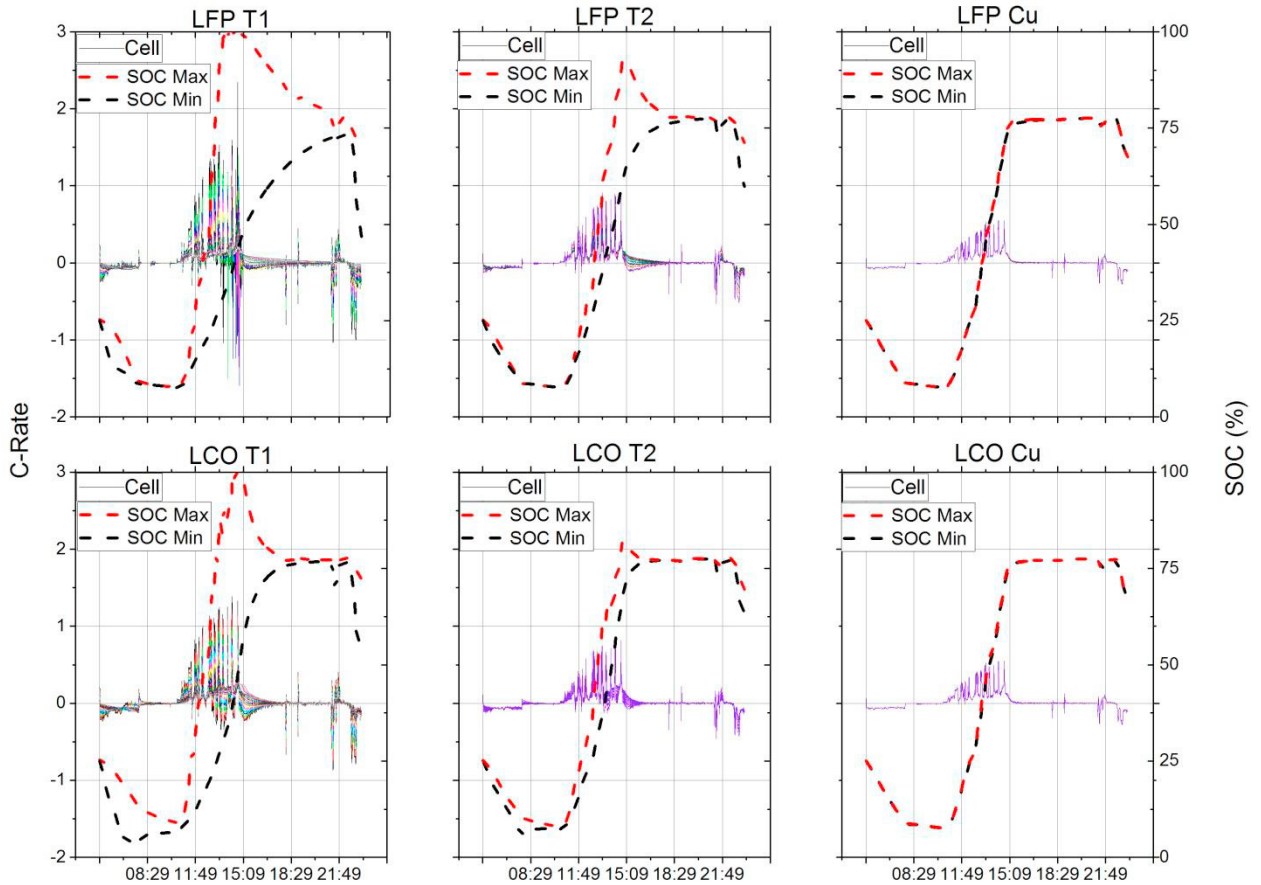
Fig. 7. Load and SOC distribution for 2 kWh and 48 V home storage systems for LFP (13s16p) and LCO (11s20p).

4.2.3. Simulation of ageing behavior for several systems and spreading cell characterizations

The results of the experiment, as well as the simulations before, have shown that the load distribution depends on the circuit design, the spread of R_{cell}, the cell chemistry and also on the number of parallel-connected cells in terms of the T1, T2 and Cu systems. Therefore we would like to show the consequences on the lifetime for different systems and scenarios.

- Normal distribution of R_{cell} in an interval of 5 % for T1 and T2
- Normal distribution of R_{cell} in an interval of 20 % for T2 and Cu
- Normal distribution of C_n in an interval of 3 % for T2

The analyzed systems were exposed to the load profile of the battery of Fig. 5 until one cell achieves an SOH of 80 %.The investigated cell formats have different lifetimes. Therefore the ageing process is for comparison normalized until EoL is achieved under test conditions for a single cell of each format (regime: 1 C CC charge and discharge; 100 % Depth of Discharge). The result is given in Fig. 8, which presents the arithmetic mean SOH of the systems over the normalized lifetime.
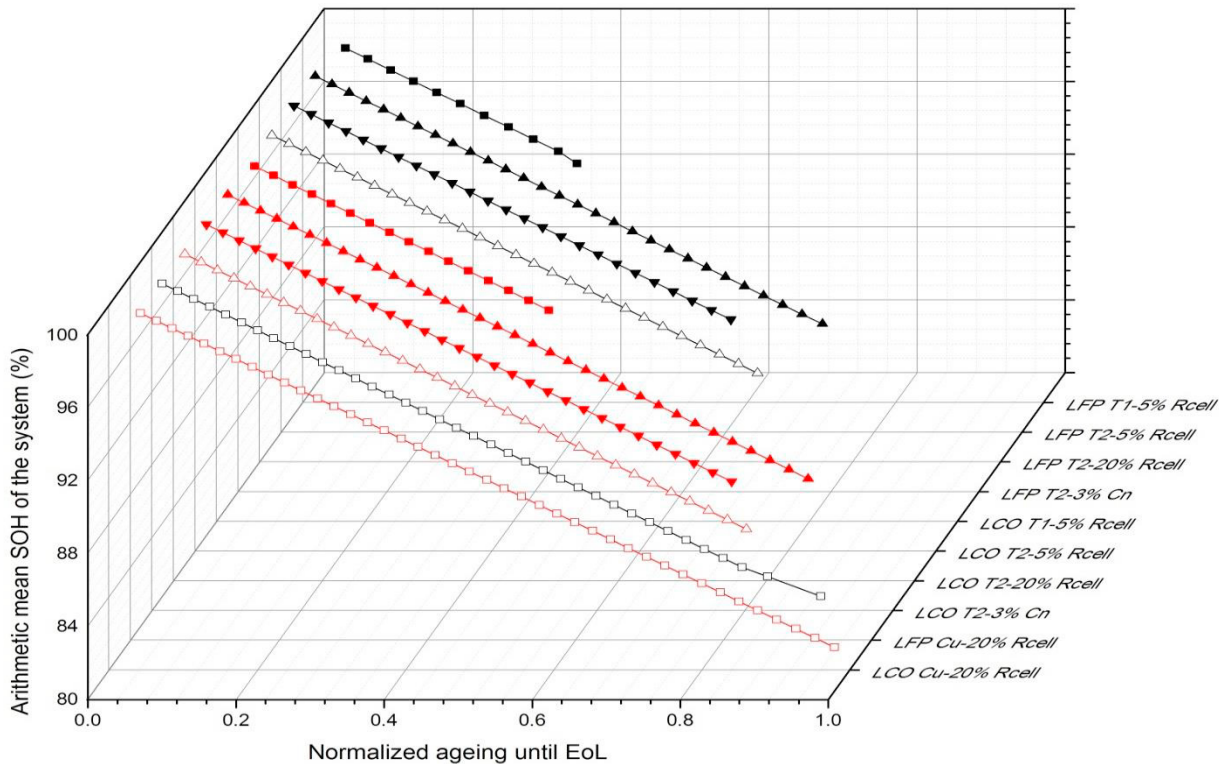
Fig. 8. Normalized lifetimes in form of the arithmetic mean SOH for several systems and scenarios of spreading cell characterizations within 2 kWh home storage systems.

It can be seen that the T1 systems with a spread of 5 % have the shortest lifetimes (LFP: 0.21; LCO: 0.45), whereas the T2 systems with the same spread achieves a lifetime, which is approximately 72-82 % of the lifetime of a single cell under test conditions. The spread of 20 % for R_{cell} reduces the lifetime of the LFP T2 system to 65 %, whereas the lifetime of the LCO T2 is only reduced from 82 % to 75 %. Regarding the spread of C_n of 3 %, it has no further influence and the same lifetimes as in the scenario of a 5 % R_{cell} spread are achieved. The Systems, which use Cu as current collector in the scenario achieve the longest lifetimes from 93 % to 97 %.

5. Discussion

The simulations and the experiments have shown that the impacts on the load distribution and the lifetime depend on the circuit design, as well as the cell chemistry.
First of all the T1 systems achieve a very high asymmetric load distribution, in which deviations in form of different R_{cell} and $R_{transfer}$ have no influence on the single cell load . The load distribution is more influenced by the circuit design. Herein with rising number of parallel-connected cells, the differences between the single cell loads increase (see Fig. 6). The analysis of the ageing behavior has shown that those systems achieve shorter lifetimes. Single cells age faster and reduce the performance of the system.

The T2 systems achieve a very high level of symmetric load distribution for low numbers of parallel-connected cells (≤4), which is nearly the load distribution in a system, which use Cu as current collector, or current collectors with large cross-sections (see Fig. 5 and Fig. 6). With higher numbers of parallel-connected cells, asymmetries in the load distribution also occur but in comparison to the T1 systems it's reduced. Regarding the results of the simulated load distribution for the 11s20p LCO T2 system, this kind of improved circuit design achieves nearly similar results like the ideal LCO Cu system (see Fig. 7).

Steel has a very low electrical conductivity, but due to the circuit design, the influence of R_{inter} was reduced and the load distribution depends more on the spread of R_{cell} and the cell characteristic. Cascaded parallel-connected modules in form of the T2 system design (e.g. four 1s4p T2 modules, which are connected in terms of the T2 system with each other; 4x1s4p $\rightarrow$ 16 cells in parallel) can gain battery modules with high numbers of parallel-connected cells with less asymmetric load distribution. Herein high cross-sections are not necessary to reduce influences of low electrical conductivities in battery modules. Material saving in the design of the current collector could be achieved, with less limitation in the number of parallel-connected cells.

It has been shown, that different SOC due to asymmetric load distribution cause high C-Rates in both charge directions in the LFP T1 system, whereas this is not the case in the LCO T1 system. The ageing simulation has shown also, that different SOC due to normal distributed R_{cell} reduce the lifetime of the LFP systems more than for the LCO systems. It can be explained by the differences in the dU_{OCV}/dQ characteristics for both cells. In a SOC area of 90-100 % the voltage curve of LFP has a very high slope, whereas in the LCO system this slope is much lower. Differences in the SOC cause different U_{OCV}, which have to be compensated by I_{cell} due to Kirchhoff's laws. Herein it is important that the energy management system considers the SOC of a home storage system during periods in which the PV power is very high. It has also to take the cell characteristics into account and run the SOC of the battery system in a status, which reduce deviations in the U_{OCV} due to different SOC to avoid high C-Rates within the parallel connection.

Furthermore the arithmetic mean SOH of the LCO T2 (5 % spread of R_{cell}) system is at EoL nearly to 82 %, which shows a relative symmetric ageing behavior within the battery module. The lifetime of this system is also only approx. 10 % less than the LFP Cu system.

In general spreads of $R_{transfer}$ has a low influence on the load distribution within welded battery systems, because of the higher electrical resistance of the cell. It can be different, if other cell formats are used (e.g. pouch format, hard case format) and also other connection techniques like screws with higher electrical contact resistances. A spread of 3 % for C_n has also a low influence but could increase if it's rising.

6. Conclusion

The main of this study was to show influences in load distribution and ageing within parallel-connected cylindrical cells in battery home storage systems, which are built up by using resistance spot welding. It has been shown that spreads in the internal cell resistance have a higher influence in those modules than deviations in the electrical contact resistance. An improved circuit design can compensate the high electrical resistance of thin nickel-strips and achieves the same symmetric load distribution of systems, which use copper as current collector or current collectors with high cross-sections for low numbers of parallel-connected cells. For higher numbers of parallel-connected cells a combination of improved circuit design and cascade architectures is proposed. The ageing level is also symmetric in this type of circuit design, which improves the performance of the battery system.

In the case of deviated SOC within a battery module, the voltage characteristic of the cell chemistry has a high impact on the load distribution and the lifetime of the system. Energy management systems of PV home storage systems have to take this into account to avoid high fluctuations in the single cell load.

Acknowledgements

References

[1] S. Kamalisiahroudi, J. Huang, Z. Li, and J. Zhang, "Study of Temperature Difference and Current Distribution in Parallel-Connected Cells at Low Temperature," Int. J. Electr. Comput. Energ. Electron. Commun. Eng., vol. 8, no. 10, pp. 1471–1474, 2014.

[2] T. Bruen and J. Marco, "Modelling and experimental evaluation of parallel connected lithium ion cells for an electric vehicle battery system," J. Power Sources, vol. 310, pp. 91–101, 2016.

[3] R. Gogoana, M. B. Pinson, M. Z. Bazant, and S. E. Sarma, "Internal resistance matching for parallel-connected lithium-ion cells and impacts on battery pack cycle life," J. Power Sources, vol. 252, pp. 8–13, 2014.

[4] M. Fleckenstein, O. Bohlen, and B. Bäker, "Aging effect of temperature gradients in Li-ion cells experimental and simulative investigations and the consequences on thermal battery management," World Electr. Veh. J., vol. 5, no. 2, pp. 322–333, 2012.

[5] H. He, R. Xiong, and J. Fan, "Evaluation of lithium-ion battery equivalent circuit models for state of charge estimation by an experimental approach," Energies, vol. 4, no. 4, pp. 582–598, 2011.

[6] T. Huria, M. Ceraolo, J. Gazzarri, and R. Jackey, "High fidelity electrical model with thermal dependence for characterization and simulation of high power lithium battery cells," 2012 IEEE Int. Electr. Veh. Conf. IEVC 2012, pp. 1–8, 2012.

[7] D. U. Sauer and H. Wenzl, "Comparison of different approaches for lifetime prediction of electrochemical systems-Using lead-acid batteries as example," J. Power Sources, vol. 176, no. 2, pp. 534–546, 2008.

[8] T. Waldmann, M. Wilka, M. Kasper, M. Fleischhammer, and M. Wohlfahrt-Mehrens, "Temperature dependent ageing mechanisms in Lithium-ion batteries - A Post-Mortem study," J. Power Sources, vol. 262, pp. 129–135, 2014.

[9] G. Ning, B. Haran, and B. N. Popov, "Capacity fade study of lithium-ion batteries cycled at high discharge rates," J. Power Sources, vol. 117, no. 1–2, pp. 160–169, 2003.

[10] S. F. Schuster, T. Bach, E. Fleder, J. Müller, M. Brand, G. Sextl, and A. Jossen, "Nonlinear aging characteristics of lithium-ion cells under different operational conditions," J. Energy Storage, vol. 1, no. 1, pp. 44–53, 2015.

[11] M. J. Brand, P. a. Schmidt, M. F. Zaeh, and A. Jossen, "Welding techniques for battery cells and resulting electrical contact resistances," J. Energy Storage, vol. 1, no. 1, pp. 7–14, 2015.